Influences of Urbanization on an Afternoon Heavy Rainfall Event over the Yangtze River Delta Region

XIAOLING JIANG,[a,b,c] DA-LIN ZHANG,[b,c] AND YALI LUO[b,d]

[a] *National Institute of Natural Hazards, Ministry of Emergency Management of China, Beijing, China*
[b] *State Key Laboratory of Severe Weather, Chinese Academy of Meteorological Sciences, Beijing, China*
[c] *Department of Atmospheric and Oceanic Science, University of Maryland, College Park, College Park, Maryland*
[d] *Innovation Center Forecast and Evaluation of Meteorological Disasters, Nanjing University of Information Science and Technology, Nanjing, China*

ABSTRACT: An afternoon heavy rainfall event occurred over coastal Nantong, an area of 70–100 km downstream from the Shanghai–Suzhou–Wuxi–Changzhou city belt over the Yangtze River Delta, under the influences of weak southwesterly monsoonal flows and lake/sea breezes on 26 July 2018. An observational analysis shows the emergence of pronounced urban heat island (UHI) effects along the city belt during the late morning hours. A series of nested-grid cloud-permitting model simulations with the finest grid spacing of 1 km are performed to examine the impacts of urbanization on convection initiation (CI) and the subsequent heavy rainfall event. Results reveal the generation of lake breezes and warm anomalies in the planetary boundary layer along the city belt and low-level convergence, thereby inducing upward motion for CI. The southwesterly flows of the monsoonal warm–moist air, enhanced by the UHI effects along the city belt, allow the development of convective cells along the city belt, some of which merge with convective clusters during their downstream propagation, and the ultimate generation of several distinct heavy rainfall centers by local convective clusters over coastal Nantong where atmospheric columns are more moist and potentially unstable under the influences of sea breezes. Sensitivity simulations show small contribution of Nantong's UHI effects to the heavy rainfall event. The above findings help elucidate how the UHI effects could assist the CI in a weak-gradient environment, and explain why urbanization can contribute to increased downwind mean and extreme precipitation under the influences of favorable regional forcing conditions.

SIGNIFICANCE STATEMENT: The urban heat island (UHI) effects tend to produce more rainfall on its downwind side than that on the other sides, but alone could hardly account for the generation of heavy rainfall. This study examines the influences of the UHI effects associated with a city belt over the Yangtze River Delta on generating an afternoon heavy rainfall event over coastal Nantong that is 70–100 km downwind from the city belt. Results show (i) the downwind advection of the UHI effects; (ii) the initiation of convective storms along the city belt, and their subsequent downstream propagation, leading to the generation of heavy rainfall over Nantong; and (iii) an important role of sea breezes in generating the heavy rainfall event.

KEYWORDS: Heat islands; Convective storms; Sea breezes; Lake effects; Precipitation; Cloud resolving models

---

1. Introduction

Urbanization could produce significant influences on local precipitation, i.e., with more rainfall over urban regions and on the downwind side (e.g., Changnon 1968; Shepherd and Burian 2003; Lei et al. 2008; Niyogi et al. 2011). Earlier studies suggest that urbanization could lead to 5%–25% increases in rainfall, particularly within 50–75 km downwind of urban centers during summer months (Changnon et al. 1981). Based on a recent meta-analysis assessment of 85 studies from 48 publications, Liu and Niyogi (2019) found that mean rainfall is enhanced by 16% and 18% over cities and their (about 50 km) downwind areas, respectively. With the rapid urbanization globally, many studies focus on the impact of urbanization on local heavy rainfall changes. For example, Kishtawal et al. (2010) claimed that urbanization makes significant impacts on the increases of heavy rainfall events over urban regions in India. Niyogi et al. (2011) found that more than 60% of storms change their structures over the Indianapolis area, with only 25% over the rural regions, based on a radar-based climatology of thunderstorm cases during 2000–09 summers. Li et al. (2020) noted an increase of ~35% in hourly rainfall rate during 1981–2011 in urbanized Kuala Lumpur, Malaysia, which is about 3 times more than that in the nearby rural areas. In China, more occurrences of heavy hourly rainfall are observed on the downwind side of the Pearl River Delta (Wu et al. 2019) and the Yangtze River Delta (Jiang et al. 2020), which are the two most economically developed agglomerations in China, during the rapid urbanization period as compared to those during the preurbanization period (i.e., prior to the mid-1990s).

In contrast to climatological analysis, numerous case studies of urbanization effects have been conducted during the past two decades, especially through numerical simulations. Results show that urbanization can alter local low-level flow patterns,

---

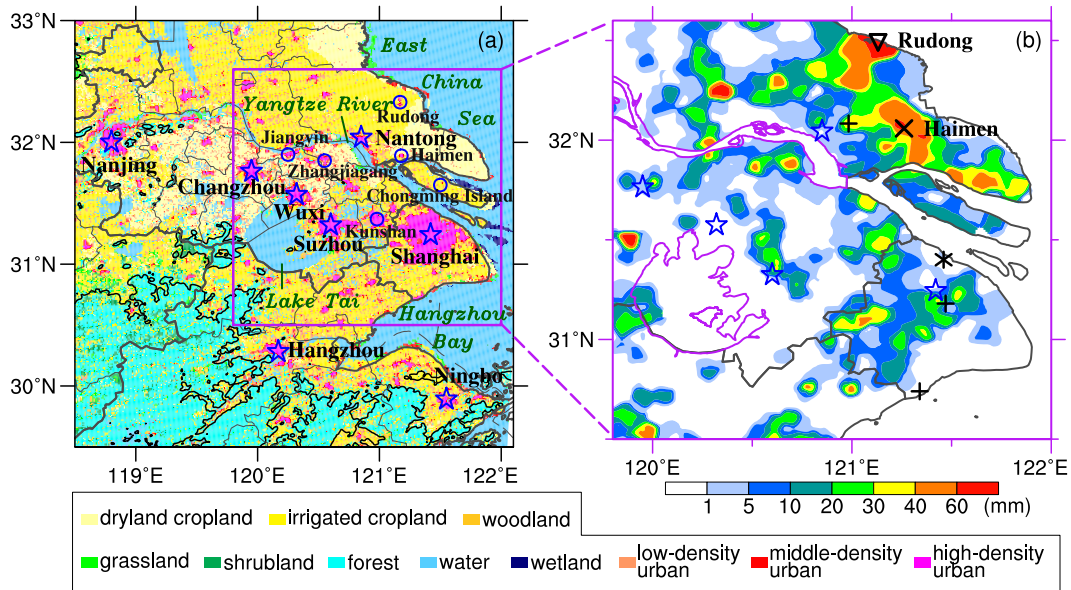*Corresponding author*: Da-Lin Zhang, dalin@umd.edu

FIG. 1. (a) The dominant land use over the YRD region in 2018 derived from the RESDC. Stars denote the locations of major cities over the YRD region, namely, Shanghai, Suzhou, Wuxi, Changzhou, Nanjing, Nantong, Hangzhou, and Ningbo (similar for the rest of the figures). Circles denote major districts, namely, the Kunshan and Zhangjiagang districts of Suzhou, the Jiangyin district of Wuxi, the Haimen and Rudong districts of Nantong, and Chongming Island of Shanghai. Thick and thin gray lines represent the borders of provinces and cities, respectively. Black lines represent the 100-m terrain elevation. The purple box represents the YRD region under study [as shown in (b)]. (b) The observed 6-h accumulated rainfall (shaded; mm) over the YRD region during the period of 1000–1600 LST 26 Jul 2018. In (b), a triangle and a cross symbol (×) denote the locations of Rudong and Haimen, two districts of Nantong, where heavy rainfall amounts of 89.2 and 69.3 mm were observed, respectively; an asterisk (*) denotes the location of the Shanghai sounding shown in Fig. 2b; the plus signs (+) denote the locations of the three wind profilers; and purple lines represent Lake Tai and the Yangtze River.

and the planetary boundary layer (PBL) structure and depth, mainly through the urban heat island (UHI) effects, facilitating convection initiation (CI) (Zhong and Yang 2015; Li et al. 2017a; Yin et al. 2020; Li et al. 2021; Sun et al. 2021). Results also show that convective storms could be strengthened over the Beijing urban region, leading to the generation of more rainfall when the UHI effects are pronounced, whereas moving storms may detour around the urban center and produce more rainfall on the lateral sides and downwind regions when the UHI effects are weak (Miao et al. 2011; Dou et al. 2015). Moreover, urban-induced rainfall may be significantly enhanced by nearby complex topography (Li et al. 2017b; Yin et al. 2020; Sun et al. 2021), and land–water contrasts (Doan et al. 2021). Urban size would also affect the downwind thunderstorm development and hence rainfall potential (Kingfield et al. 2018).

It is evident from the previous studies that the relative importance of urbanization versus various local surface forcings and environmental conditions in determining rainfall production could vary markedly among different urban regions (Zhang 2020). In general, urbanization alone could hardly produce heavy rainfall, defined herein as greater than 20 mm h^{-1} or 50 mm day^{-1} over a significant area (Li et al. 2017c), because the generation of heavy rainfall involves the synergetic interaction between urban-induced circulation and some external forcings such as local topography and land–water contrasts

even in the presence of ample moisture (Zhang 2020; Chen et al. 2022). Despite the growing interest in the impact of urbanization on heavy rainfall during the recent years, few case studies have been performed to understand the generation of heavy rainfall under the influences of multiple UHIs of different sizes coupled with land–water contrasts. Thus, the purpose of this study is to fill in this gap by exploring the impact of multiple UHIs on a heavy rainfall event that occurred in the northern portion of the Yangtze River Delta (YRD), located in coastal East China. Specifically, the YRD has undergone rapid urbanization since the early-to-middle 1990s (Liang and Ding 2017; Jiang et al. 2020). The YRD urban agglomeration consists of several metropolitan areas, such as Shanghai, Suzhou, Wuxi, Changzhou, Nanjing, and Hangzhou (see Fig. 1a for their locations). Of relevance to this study is that Suzhou, Wuxi, and Changzhou, often referred to as Suzhou–Wuxi–Changzhou (SXC) in China, are almost bonded to form a city belt on the south of the Yangtze River and the west of Shanghai. Nantong, relatively a smaller city located at the northern shore of the Yangtze River, is 70–100 km away from the city belt and usually on the downwind side during the summer (southwesterly) monsoon period (Fig. 1a).

Rapid urbanization over the YRD region has significantly changed its regional climate. Liang and Ding (2017) found that Shanghai became like a "rain island" with increasing
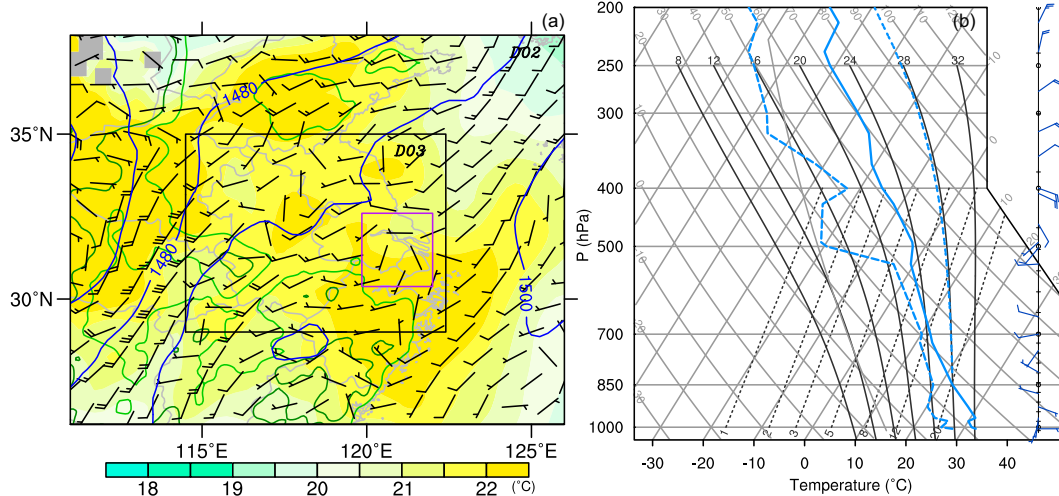
FIG. 2. (a) The NCEP-FNL reanalysis at 0800 LST 26 Jul 2018: geopotential height (blue lines; gpm) and temperature (shaded; °C) at 850 hPa, and horizontal winds (a full barb is 4 m s^{-1}) at 900 hPa. Light and dark green lines denote the 100- and 500-m terrain elevation, respectively. Nested model domains used for the WRF simulations with a grid spacing of 3 km (D02) and 1 km (D03), respectively, are marked by black rectangles. The purple rectangle represents the YRD region used for regional analysis in this study. (b) A sounding taken at the Shanghai observatory (see Fig. 1b for its location) at 0800 LST 26 Jul 2018, but with no data available above 200 hPa. A full barb is 4 m s^{-1}.

trends in heavy rainfall over the major urban area during the recent urbanization period (i.e., 1981–2014). A climatological analysis by Jiang et al. (2020) revealed substantial increases in heavy rainfall over the YRD urban agglomeration, including Shanghai and SXC, with a downstream high value in Nantong, during the rapid urbanization period (i.e., 1997–2018), as compared to the preurbanization era (i.e., 1975–96). The regional climate and rainfall over the YRD region could be significantly influenced by local land–water contrasts, complex topography (albeit low elevated), and the interaction of urban-induced circulations between the clustered cities. In this regard, Zhang and Chen (2014) noted the downstream enhancement of the UHI effects over Wuxi by that over Suzhou, a process first found by Zhang et al. (2009), through a numerical modeling and observational case study. By comparing model simulations with and without urban regions, Wan et al. (2013) detected more occurrences of rainfall on the downwind side of the Shanghai–SXC city belt. Similarly, a numerical simulation of urbanization effects by Zhu et al. (2015) shows that the presence of Shanghai increases surface temperature and the PBL depth on its downwind city, Kunshan (see Fig. 1a for its location). Since significant increases of heavy rainfall were detected over Nantong from a 44-yr climatological analysis [see Figs. 3 and 7 in Jiang et al. (2020)], we may conjecture that the increased rainfall was closely related to the urbanization associated with the city belt on the south of the Yangtze River. To validate this hypothesis, the heavy rainfall event of 26 July 2018 over coastal Nantong with CI occurring along Shanghai–SXC is simulated. This event also contributed to the climatological high rainfall values over Nantong shown in Jiang et al. (2020). The objectives of this study are to (i) document the large-scale environment in which the heavy rainfall event occurred, including the CI and subsequent storm development; (ii) obtain a reasonable cloud-permitting

simulation of the heavy rainfall event, as verified against detailed observations; and (iii) examine to what extent the heavy rainfall event over coastal Nantong was determined by the upstream urban clusters, i.e., the Shanghai–SXC city belt, and the urbanization of Nantong as well as local coastal flows.

The next section provides an overview of the case. Section 3 describes the model configurations and experiment design, and shows verifications of the model simulation against various observations. Section 4 shows a detailed analysis of the impacts of urbanization on CI and the subsequent heavy rainfall event over Nantong. Section 5 presents three sensitivity experiments due to different urbanization components and examines the overall, upstream, and Nantong-related urban impacts on the heavy rainfall production. A summary and conclusions are given in the final section.

2. Case overview

The heavy rainfall event of concern took place on the north of the Yangtze River mainly during the period of 1000–1600 LST (local standard time = UTC + 8 h) 26 July 2018. During this period, there were seven automated weather stations (AWSs) that recorded the hourly rainfall rates of more than 50 mm h^{-1}. A 6-h accumulated rainfall maximum of 89.2 mm was recorded in Rudong, which is located to the northeast of the Nantong city (see Fig. 1b for its location), with an hourly amount of 66.7 mm at 1500 LST. Another 6-h accumulated rainfall center of 69.3 mm, with an hourly amount of 54.1 mm at 1400 LST, took place in Haimen, which is located to the east of the Nantong city (Fig. 1b).

Although significant rainfall also occurred near Hangzhou and Ningbo, the associated processes are not discussed herein because they are not related to the heavy rainfall event of interest. In addition, the urban impacts of Nanjing, a large city
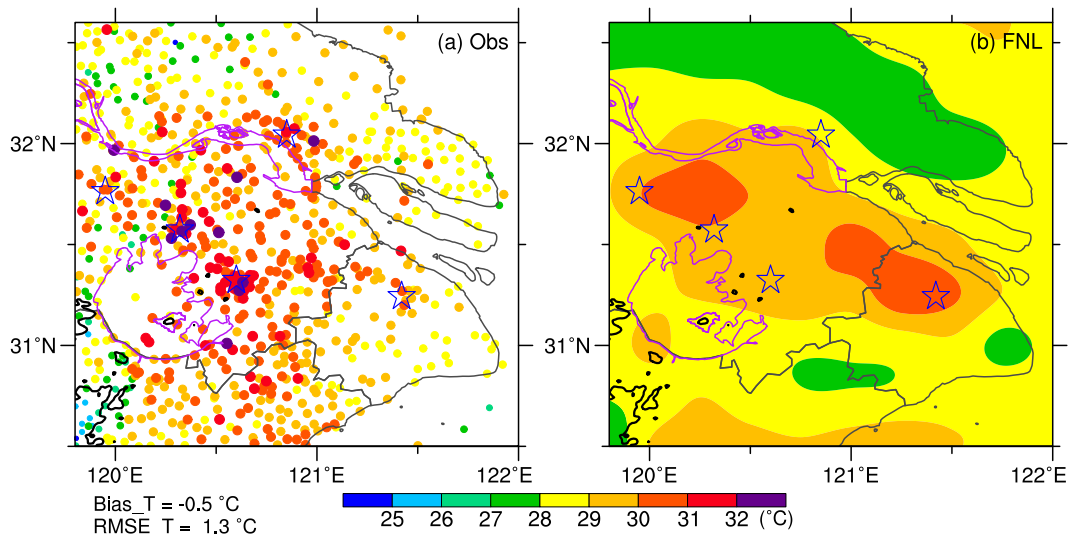
FIG. 3. Comparison of (a) the AWSs observed to (b) the NCEP-FNL surface ($z = 2$ m) temperature at 0200 LST 26 Jul 2018. Black lines represent the 100-m terrain elevation.

to the west of Changzhou, are ignored because of the occurrence of little rainfall nearby and little influences on the heavy rainfall event under study.

Figure 2a shows the large-scale flows in the lower troposphere at 0800 LST 26 July 2018, which was about 2 h prior to the CI of the heavy rainfall event under study. The YRD region, illustrated by a purple box, was situated over the alluvial plain with mountains of 100–500-m altitude to the south. The large-scale environment was influenced by a subtropical high, centered in the west North Pacific basin, and a southwesterly monsoonal flow, with a short-wave trough at 850 hPa on the northwest of the box. At the regional scale, the YRD was dominated by a weak shear line with flows of 2 m s^{-1} at 900 hPa that appears to be associated with the trough at 850 hPa [see Yao et al. (2020) for a detailed description of the characteristics of shear lines occurring in East China]. In addition, the 850-hPa thermal field exhibited a weak gradient, varying in the range of 21°–22°C over the YRD region. An 0800 LST sounding taken at Shanghai, as given in Fig. 2b, exhibits wind speeds of less than 4 m s^{-1} up to 500 hPa, and conditional instability with large convective available potential energy (CAPE) of about 3558 J kg^{-1}. It is evident that the heavy rainfall event took place under a weak-gradient environment with weak flows and significant conditional instability. This is typically favorable for the occurrence of the enhanced UHI effects (Changnon 1969; Shepherd 2005; Zhang 2020).

3. Model description and verification

a. Model description

The heavy rainfall event is simulated herein using the Weather Research and Forecast (WRF, v3.9.1) Model. Two-way interactive, triply nested domains with the respective grid spacing of 9, 3, and 1 km are used. The innermost two domains (i.e., D02 and D03), as shown in Fig. 2a, cover the (x, y) areas of 1299 km × 1254 km and 700 km × 652 km, with grid

points of 433 × 418 and 700 × 652, respectively. The outermost domain (i.e., D01) covers an (x, y) area of 2403 km × 2205 km with 267 × 245 grid points (not shown), and it is centered at 31°N, 118°E. A total of 57 sigma levels are used in the vertical. The following model physics schemes are used for all the domains: (i) the WRF double-moment 6-class microphysics scheme (Lim and Hong 2010); (ii) the RRTMG schemes for both shortwave and longwave radiative flux calculations (Lacono et al. 2008); (iii) the MYJ PBL scheme (Mesinger 1993; Janjić 1994); (iv) the Monin–Obukhov scheme for the surface layer (Zhang and Anthes 1982; Janjić 2002); (v) the unified Noah land surface scheme (Chen et al. 2011); and (vi) the single-layer urban canopy model (Chen et al. 2011). Only in the outermost domain, is the Kain–Fritsch cumulus parameterization scheme (Kain 2004) activated. The above physics options have been often used to simulate the UHI effects and associated heavy rainfall events (e.g., Zhang et al. 2011; Wan et al. 2013; Yin et al. 2020).

To better represent the effects of urbanization, the land-use dataset in 2018 with 1-km grid spacing from the Resources and Environment Scientific Data Center (RESDC), the Chinese Academy of Sciences (http://www.resdc.cn/data.aspx?DATAID=98) is adopted and transferred to the format used in the WRF (Fig. 1a). The dataset includes 25 land-use types, such as builtup lands with different degrees of urbanization, croplands for different uses, and it has been widely used in the previous studies of land resources surveys (e.g., Liu et al. 2014; Li et al. 2015) and urban–rainfall relationship (Wu et al. 2019; Jiang et al. 2020). The National Centers for Environment Prediction's final (NCEP-FNL) reanalysis data with 0.25° grid spacing at 6-h intervals from 0200 LST 26 July 2018 are used as the model initial conditions and the lateral boundary conditions.

During our preliminary experimentation, the NCEP-FNL reanalysis, used as the model initial conditions, underestimates the nocturnal UHI effects along the city belt over the YRD region,
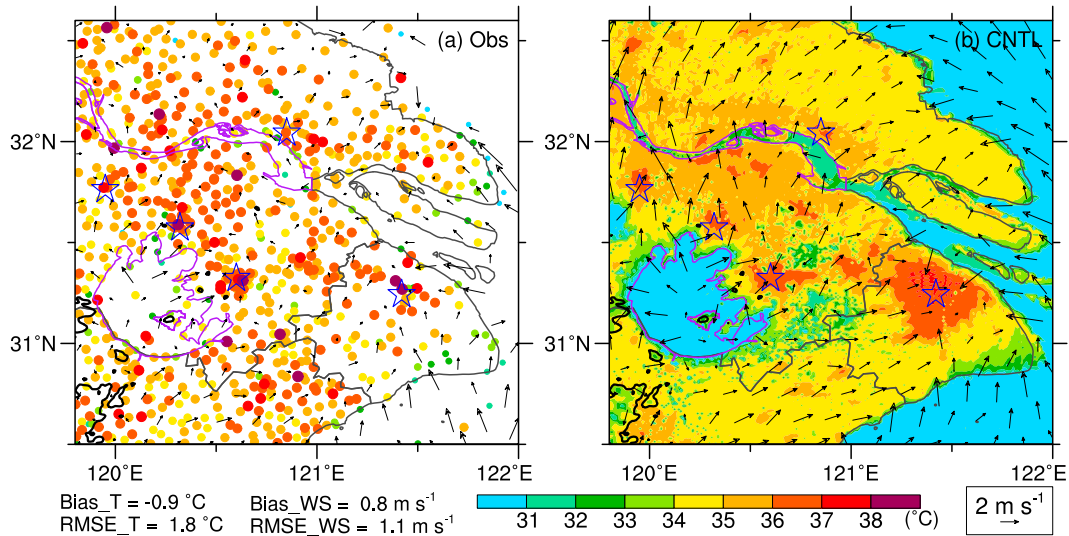
FIG. 4. Comparison of (a) the AWSs observed to (b) the 2-h simulated surface ($z = 2$ m) temperature and ($z = 10$ m) horizontal wind vectors, valid at 1000 LST 26 Jul 2018.

which may be attributed to its relatively coarse resolution. As a result, the simulated CI during late morning hours is significantly delayed, as verified against the observed. For example, Fig. 3 compares the observed surface temperatures from the AWSs to the FNL reanalysis at 0200 LST 26 July (i.e., the model initial time). Strong UHI effects were detected over the cities, especially near the urban centers of Suzhou, Wuxi, and Nantong, where the observed surface temperatures exceeded 32°C that were 3°–4°C warmer than the rural areas. The UHI effects over Shanghai were weaker due likely to the cold air advection in the lowest 100-hPa layer from the ocean surface (Fig. 2b). In contrast, the FNL reanalysis shows the surface temperatures of about 30°C along the Shanghai–SXC city belt, which is about 2°C cooler than the observed (cf. Figs. 3a,b). On average, the FNL data are about 0.5°C colder than the observations over the YRD region. Locally, the UHI centers in the FNL data are notably deviated from those of the observed, especially over Suzhou and Wuxi (cf. Figs. 3a,b).

To minimize the influences of the underestimated UHI effects in the initial condition, the four-dimensional data assimilation (FDDA) of Stauffer and Seaman (1990, 1994) and Stauffer et al. (1991) is applied by activating the surface observation nudging (Liu et al. 2008) in the innermost 1-km grid-spacing domain (i.e., D03) from 0200 to 0800 LST 26 July. Hourly surface observations of temperature, moisture, and winds at about 7400 AWSs are used for this purpose. This dataset has been quality controlled and archived by the National Meteorological Information Center (NMIC) of China, and widely used for regional weather and climate studies (e.g., Yu et al. 2010; Luo et al. 2016; Chen et al. 2018). The innermost domain is then integrated freely for 8 h (i.e., from 0800 to 1600 LST 26 July). The simulated CI occurs 2.5 h after turning off the observation nudging, i.e., near 1030 LST. In addition, the analysis nudging (Stauffer and Seaman 1994; Liu et al. 2008) is applied to the outer two domains (i.e., D01 and D02) throughout the entire integration period in order to minimize error growth in the larger-scale flows.

b. Model verification

In this section, we verify the 8-h simulation of the heavy rainfall event against various observations (e.g., surface analyses, and radar observations). Statistically, regional mean difference and root-mean-square error (RMSE) in surface temperature between the simulation and observations (i.e., simulation minus observation) is −0.9° and 1.8°C, respectively (Fig. 4), valid at 1000 LST. Note that the cold bias inherited from the FNL reanalysis, as mentioned before, persists into the simulation beyond 1000 LST. This is because numerical models tend to "forget" quickly the nudged surface-layer temperature and wind in a stable PBL once free integration starts. Moreover, some differences can be expected since the observed surface temperature and wind are obtained at the 2- and 10-m level, respectively, whereas the simulated are defined as the surface-layer average.

Next, more attention will be given to ascertaining how well the WRF model reproduces the CI along the city belt on the south and subsequent generation of the heavy rainfall centers on the north of the Yangtze River. Figure 4 compares the AWS-observed surface temperatures and horizontal winds from the 2-h simulation, valid at 1000 LST that was about 0.5 h prior to the CI. Surface temperatures higher than 37°–38°C were observed at Shanghai, Suzhou and Wuxi, and the other urban regions, with the urban–rural differences of 3°–4°C (Fig. 4a). This shows the presence of the UHI effects prior to CI. Despite the presence of the previously mentioned cold bias, the simulated surface temperature anomalies agree reasonably well with those observed, with warm anomalies centered over the urban areas of Shanghai, Suzhou, Wuxi, and Changzhou, as well as Nantong and other small towns (cf. Figs. 4a,b). In addition, the simulation produces systematically positive wind speed biases with a regional average of 0.8 m s^{-1} compared to the observations, which could be attributed partly to the interpolation of surface winds from the model surface layer of
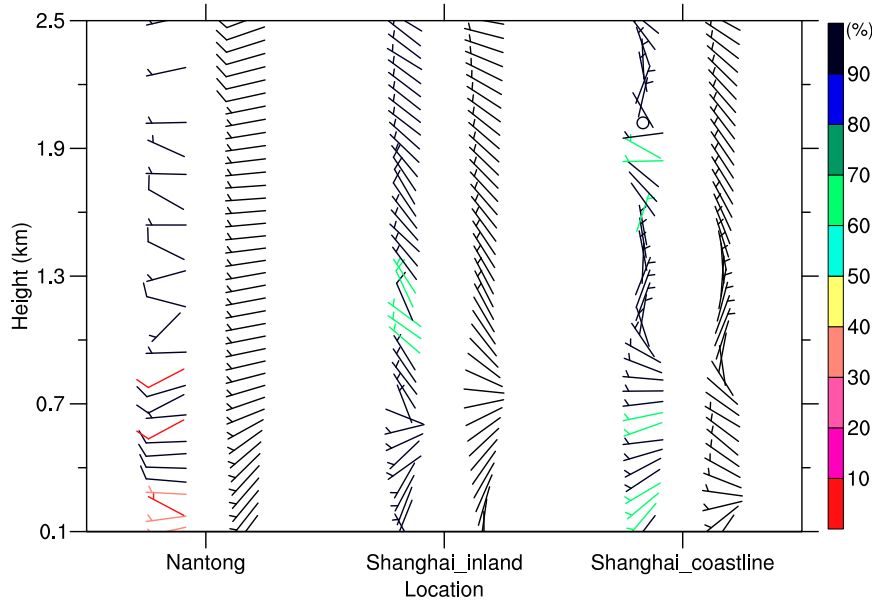
FIG. 5. Comparison of the observed (left column of barbs) and the simulated horizontal wind vectors (right column of barbs) in the lowest 2.5-km layer at three wind profiler stations (see Fig. 1b for their locations), valid at 1000 LST 26 Jul 2018. Colors are used to show the credibility (%) of the observed winds. A full barb is 4 m s^{-1}.

45–50-m depth to the 10-m level. However, both the simulation and observations show weak sea breezes that begin to develop along the coastal regions, as indicated by onshore surface winds along the coastline.

Figure 5 compares the vertical profiles of horizontal wind vectors in the PBL between the real-time Doppler radar-based wind profiler data and the simulation at Nantong and Shanghai (see Fig. 1b for their locations). The wind profiler data were collected and quality controlled by the China Meteorological Administration (CMA) with vertical spacings of 120 and 60 m at Nantong and Shanghai, respectively, and they have been assessed to be reliable for general applications (Liu et al. 2020). In general, both the observed and simulated winds in Nantong are westerly and about 2–4 m s^{-1} in the lowest 2.5-km layer. Some notable differences between them are mainly in the lowest 700-m layer, where the credibility of the wind-profiler data is low (<30%). For regions in Shanghai, including both inland and coastline, the simulated winds veer from southwesterly to northwesterly with height, which agrees well with the observations. In particular, the simulation could reasonably reproduce the directional transition from westerly winds below 0.8 km to northerly winds between 0.8 and 1.6 km and northwesterly above at the coastline in Shanghai.

After verifying the UHI effects and horizontal winds in the PBL at 1000 LST, Fig. 6a shows the initiation of convective cells less than one hour later, slightly downstream from Shanghai, Suzhou, and Wuxi. It is evident that sea and lake breezes assisted in the storm formation near Shanghai and the latter two cities, respectively. Note the development of weak convergence between the Yangtze River and the city belt,

where towns of Jiangyin and Zhangjiagang are located (see Fig. 1a for their locations). By 1200 LST, CI occurred at Changzhou and Nantong with scattered convective cells developing along the above convergence zone (Fig. 6c). More pronounced convergence zone occurred near Nantong as sea breezes progressed inland. Note also that all the convective cells, though scattered, tended to produce significant convergence along (evaporatively driven) cold outflows on the north of the city belt, except near Nantong where new convection just developed at the sea breeze front. Some cells dissipated shortly after their formation, while the others were merged into clusters under the influences of the sea breezes and cold outflows. Two more pronounced convective clusters with one near Haimen and the other moving toward Rudong, denoted by "E" and "N," respectively, were locally formed at 1400 LST (Fig. 6e). It was the two clusters with a lifetime of 2–3 h that produced heavy rainfall in the coastal Nantong region (cf. Figs. 1b and 6e), because the individual convective cells were generally short-lived, i.e., less than 1 h. The short-lived nature could be attributed to the presence of weak vertical shear such that the convective cells tended to remain locally by the outflow-induced circulation and then dissipated in the stable atmospheric columns above cold pools (Rotunno et al. 1988). The two clusters began to dissipate shortly after. By 1600 LST, most of the Nantong regions were distributed with widespread outflows in the surface layer and remnant clouds with weak rainfall from the dissipating clusters (Fig. 6g). By comparison, sea breezes along the coastline and the Hangzhou Bay played an important role in modulating the urban-induced circulations throughout the 8-h integration period.
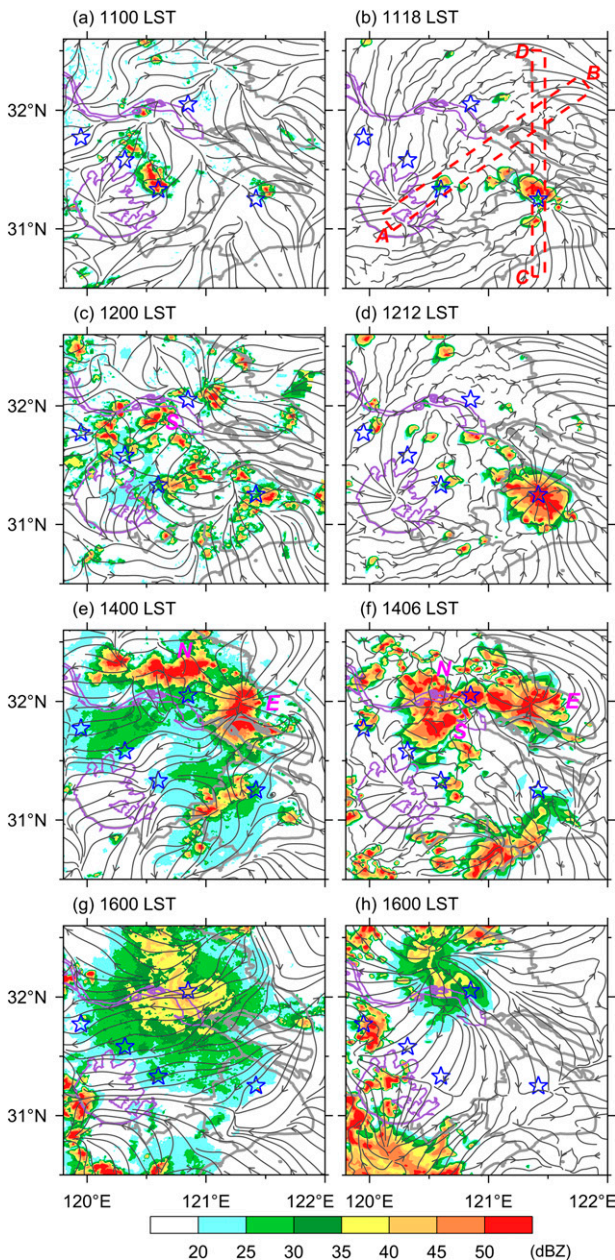
FIG. 6. Horizontal maps of the (a),(c),(e),(g) observed and (b),(d),(f),(h) simulated composite radar reflectivity (shaded; dBZ), superimposed with surface ($z = 10$ m) streamlines. Letters, "E," "N," and "S," denote three heavy-rain-producing convective clusters mentioned in text. Two elongated rectangles A–B and C–D in (b) denote the area-averaged vertical cross sections used in Figs. 9a and 9b, respectively.

A comparison of Figs. 6a–d shows that the model simulates reasonably well CI on the downstream side of the Shanghai–SXC city belt, albeit 15–30 min later than the observed. The effects of sea and lake breezes on the CI are also well simulated. The delayed CI results in the delayed formation of cluster S between Wuxi and Nantong (cf. Figs. 6c–f). The delayed CI could be attributed partly to the typical model spinup problems, and

partly to the cold biases of surface temperature (Fig. 4) inherited from the FNL reanalysis. In addition to the formation of cluster S, the model mimics the formation of new convective cells ahead of dissipating cells on the downstream side of the city belt, a characteristic of discrete propagation. As will be seen in section 4, cluster S fails to move northward across the Yangtze River due to the presence of a shallow stable layer over the water surface; similarly for the observed. So, cluster S does not contribute directly to the heavy rainfall accumulated but indirectly through its cold outflows to the CI and convective organization on the north of the Yangtze River. Despite the delayed CI, the model also reproduces the local formation of clusters E and N around the Nantong city at 1406 LST, although they appear to be more loosely organized than the observed (cf. Figs. 6e,f). Clusters E and N exhibit significant dissipation with divergent outflows by 1600 LST, albeit at some distance on the northwest of the observed (cf. Figs. 6g,h). Of significance is that few convective cells are present along the city belt and Shanghai by 1600 LST, which is consistent with the observed. In addition, the model reproduces the sea-breeze-induced convective cells/clusters on the southwest of Shanghai, and a large multicell cluster around Hangzhou by 1600 LST (cf. Figs. 6e–h). In contrast, few convective cells appear offshore in both the observation and simulation during the 8-h integration period, due to the presence of stable atmospheric columns over the ocean surface under the control of the subtropical high.

Figure 7 shows the simulated 6-h accumulated rainfall ending at 1600 LST. In general, both the distribution and magnitude of the simulated rainfall amount compare favorably to the observed (cf. Figs. 7 and 1b). Pronounced rainfall of 40–60 mm took place primarily over the coastal Nantong region (i.e., at Haimen, Rudong, and a couple of AWSs to the northwest), near the southern bank of the Yangtze River in association with cluster S, and Shanghai, but with little rainfall occurring along the city belt (Fig. 1b). The WRF Model reproduces reasonably well the accumulated rainfall centers in the coastal region, with a heavy rainfall center near Haimen and another center near Rudong, as denoted by a blue cross and a triangle sign in Fig. 7, respectively. However, besides some position errors, the model-simulated heavy rainfall area coverages are smaller than the observed, especially at Rudong, due to the simulated clusters E and N that are more loosely organized than the observed (cf. Figs. 6e,f), as mentioned before. Perhaps, the most obvious difference is that the simulated rainfall intensity of more than 60 mm over the Nantong city is much higher than the observed. This overpredicted rainfall intensity can be traced back to the lacking formation of a storm on its east by 1200 LST (cf. Figs. 6c,d) such that the presence of local conditional instability would facilitate the generation of more rainfall than the observed at the Nantong city. (This will be further discussed near the end of section 4.) As a result, the simulated cluster E consumes more moisture that would be otherwise available for rainfall generation downstream by cluster N having a weaker intensity than the observed. All these help explain why the simulated heavy rainfall area coverage at Rudong is much smaller than the observed. Nevertheless, the model produces little rainfall along the Shanghai–SXC city belt and over a large area between the Yangtze River and Hangzhou, which agree well with the observed (cf. Figs. 7 and 1b).
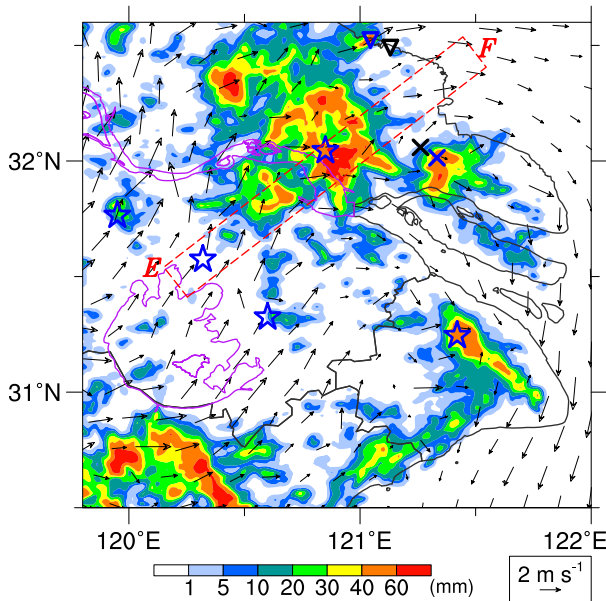
FIG. 7. Simulated 6-h accumulated rainfall during 1000–1600 LST 26 Jul 2018 (shaded; mm), superimposed by horizontal wind vectors at 900 hPa at 1100 LST 26 Jul 2018. The blue cross symbols and triangles represent the simulated locations of rainfall centers, which are compared to the observed as indicated by black signs in Fig. 1b. An elongated rectangle E–F denotes the area-averaged vertical cross section used in Fig. 11.

Figure 8 compares the time series of the simulated hourly rainfall at the two major rainfall centers (i.e., over coastal Nantong) to the observed. Haimen and Rudong received the peak hourly rainfall rates of 54.1 and 66.7 mm h^{-1}, respectively, at 1400 and 1500 LST. The heavy-rain-producing clusters moving through Haimen and Rudong lasted for less than 3 h (cf. Figs. 8, 1b, and 6e). It is evident from Fig. 8 that the model reproduces well the initiation, the peak occurrence, and the ending time of heavy rainfall at Haimen, although its peak hourly rainfall rate is about 10 mm h^{-1} smaller than the observed. Of interest is that in spite of the smaller heavy rainfall coverage, the simulated peak intensity at Rudong is closer to the observed, albeit with an hour lag in the initiation and peak intensity. The simulated weaker intensities could be attributed to the grid spacing of 1 km that is still too coarse to reproduce the needed intense updrafts for the generation of heavy rainfall (Bélair and Mailhot 2001; Yau et al. 2004).

Based on the above results, we may state that despite the presence of some model errors, the CI and subsequent storm development as well as the heavy rainfall locations are reasonably well reproduced. Thus, the model simulation can be used in the next section to explore the impact of urbanization on the CI along the city belt, and the generation of the heavy rainfall event over the Nantong region.

4. UHI impacts on the convection initiation

To help gain insight into the UHI-induced CI under the general environmental conditions, Fig. 9a shows a vertical cross
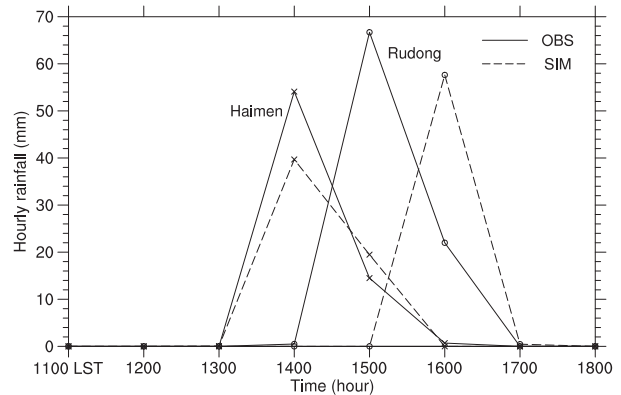

FIG. 8. Time series of the observed (solid) and simulated (dashed) hourly rainfall rates (mm h^{-1}) near Haimen and Rudong during the period of 1100–1800 LST 26 Jul 2018.

section of the equivalent potential temperature (θ_e), potential temperature (θ), temperature perturbations, and cloud water along the low-level southwesterly flow through the CI locations of Suzhou at 1030 LST, when CI just begins. Note several water bodies, e.g., associated with Lake Tai, the Yangtze River, and the East China Sea, that are characterized with lower-θ air in the lowest 500-m layer, implying that the PBL over the water surfaces are convectively stable. This helps explain why cluster S and most convective cells fail to propagate northward across the Yangtze River (cf. Figs. 9 and 6). This can also be seen from the generation of little or northward decreasing rainfall amounts to the river (Figs. 7 and 1b). In contrast, a distinct warm anomaly of more than 0.5°C in the lowest 500-m layer takes place at Suzhou (Fig. 9a), which results from its UHI effects. Although the warm anomaly is still weak at this early morning hour, the thermal-low-induced low-level convergence has induced favorable upward motion leading to the formation of cloud water, i.e., CI. Similarly, there exists a warmer and deeper temperature perturbation of more than 1.0°C in the lowest 1-km layer near the Shanghai city as compared to that at Suzhou, leading to the formation of a thicker PBL (1.5 km) and the triggering of cloud condensation with strong upward motion (Fig. 9b), and the development of intense convection (Fig. 6d).

Note that the PBL depth increases downstream, as indicated by more elevated 308–309-K isentropic surfaces from Suzhou northeastward until reaching the coastline, where maritime lower-θ air begins to intrude inland, i.e., through sea breezes (Fig. 9a). The downstream increased PBL depth results partly from the advection of monsoonal warm-moist air, and partly by the advection of the UHI effects associated with the city belt, as indicated by lower-θ columns in the lowest 1-km layer over Lake Tai but well-mixed (i.e., θ = constant) higher-θ columns on the downwind side of Suzhou. The latter is consistent with the downstream propagation of the UHI effects found by Zhang et al. (2009). It is worthwhile to mention that this increased PBL depth on the downwind side of the city belt could be a frequent regional phenomenon under the dominant control of the subtropical high with a southwesterly monsoonal flow over the YRD region. However, previous studies only paid
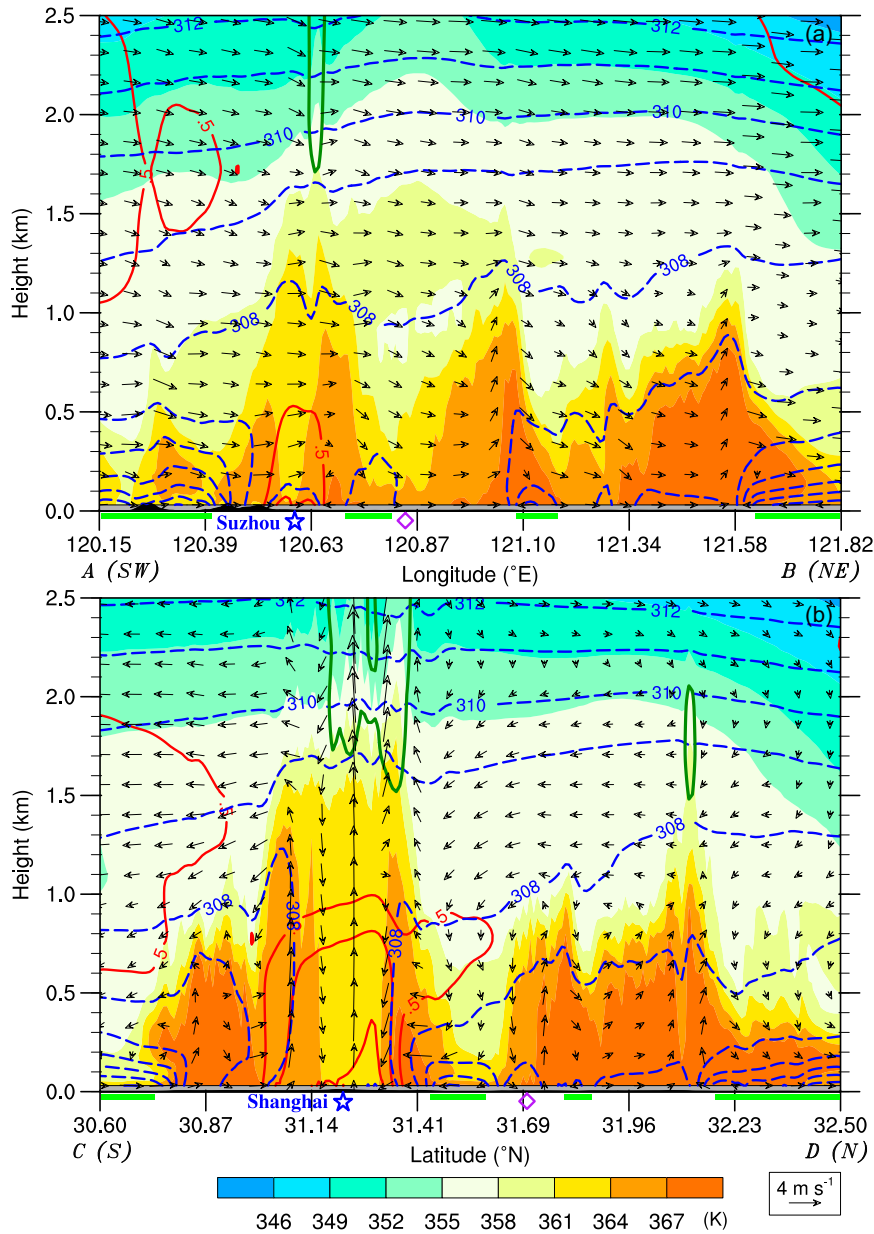
FIG. 9. Vertical cross section of the area-averaged equivalent potential temperature (θ_e; shaded; K), temperature perturbations (contoured in red starting from 0.5°C at intervals of 0.5°C), potential temperature (θ; blue dashed contours at intervals of 1 K), cloud water (dark green contours for 0.05 g kg^{-1}), superimposed with in-plane flow vectors (m s^{-1}) with vertical motion amplified by a factor of 10, along elongated rectangles (a) A–B and (b) C–D in Fig. 6b, valid at 1030 LST 26 Jul 2018. The temperature perturbations are calculated by subtracting the rural mean temperatures at the location shown by purple squares, and at altitudes above the surface. Terrain is shaded in black, with water surfaces denoted by light green bars underneath the bottom frame. Blue stars denote locations of urban areas where convection is initiated.

attention to the downstream enhancement of the UHI effects along the city belt due to the influences of westerly flows (e.g., Zhang et al. 2011; Zhu et al. 2015), as mentioned in section 1, rather than normal to it. Of importance is that several high-θ_e domes take place from Suzhou to Nantong, making this region

favorable for triggering new convection in the presence of low-level convergence. Similar signals can be detected along the cross section from Shanghai to Nantong. While relatively higher-θ_e air is distributed from Shanghai to Nantong and beyond, relatively lower-θ_e air is advected from the Hangzhou Bay to Shanghai
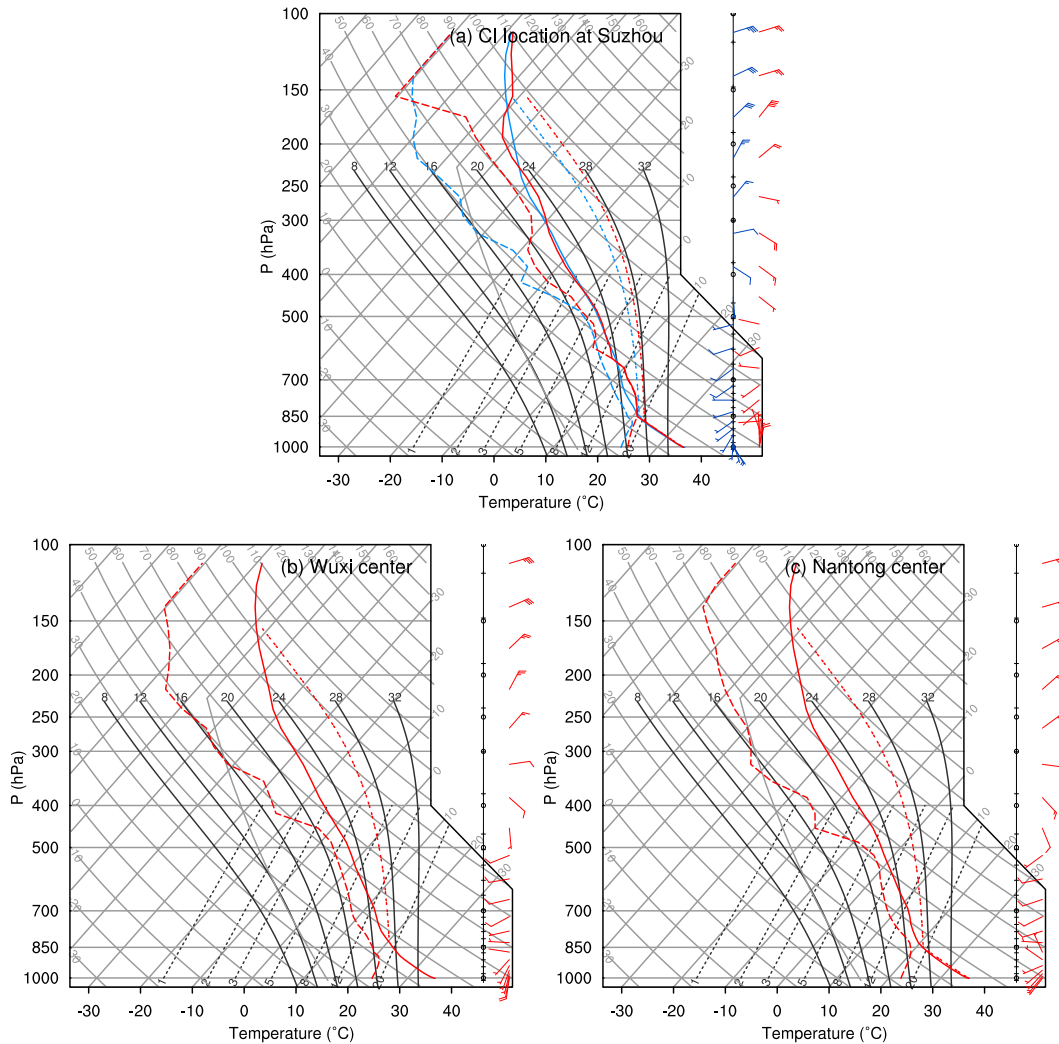
FIG. 10. Simulated soundings at (a) the CI location at Suzhou, i.e., given by a blue star beneath the frame of Fig. 9a, (b) the Wuxi city, and (c) the Nantong city, i.e., given by blue stars in Fig. 6b, valid at 1000 LST (blue) and 1100 LST (red) 26 Jul 2018. A full barb is 4 m s^{-1}. Soundings at 1000 LST at both Wuxi and Nantong are not shown because of their little differences from those at 1100 LST.

(Fig. 9b). This helps explain why convective storms do not propagate southward along the coastline from Shanghai in both the observation and simulation (Fig. 6).

To see further the impact of the UHI effects on CI, the simulated soundings, taken at the warm-anomaly center at Suzhou at 0.5 h prior to (i.e., 1000 LST) and after (i.e., 1100 LST) the CI, respectively, are given in Fig. 10a, showing that the PBL is well mixed up to 850 hPa, due to the solar heating enhanced by the UHI effects, with weak vertical shear in the lower half of the troposphere prior to the CI. This sounding also exhibits the existence of dry air above 500 hPa, which accounts for the source of evaporatively driven downdrafts causing the generation of surface cold outflows shown in Fig. 6. This preconvective sounding reveals the presence of significant conditional instability with large CAPE. By 1100 LST, the CI is triggered as the air at the urban PBL top reaches saturation, and then an intense updraft

driven by latent heat release begins to develop, leading to the formation of clouds in the 850–600-hPa layer (cf. Figs. 10a and 9a). In contrast, the air near the urban PBL top at the Wuxi city does not reach saturation even at 1100 LST, which explains why its CI occurs about one hour later than that at Suzhou (cf. Figs. 10a,b and 6b,d). Similarly, CI does not occur near Nantong, even though its vertical column is conditionally unstable, until convectively generated outflows arrive there (cf. Figs. 10c and 6f).

To help understand why CI occurs along the city belt but heavy rainfall takes place over the Nantong region, Fig. 11 shows time series of the most unstable CAPE (MUCAPE; i.e., from the most unstable air parcel in the lowest 300-hPa layer), surface wind speeds, and specific humidity along the rectangle E–F, as given in Fig. 7, i.e., from where CI first takes place near Wuxi to where heavy rainfall occurs at Nantong,
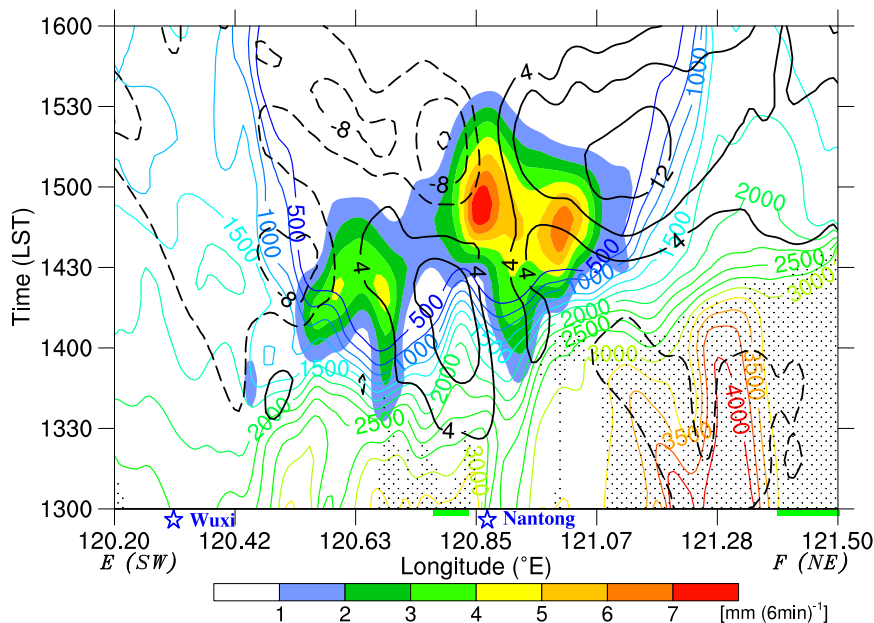
FIG. 11. Time series of the area-averaged rainfall rate [shaded; mm (6 min)$^{-1}$], MUCAPE (colored contours increasing in magnitude from blue to red; J kg^{-1}), in-plane surface ($z = 10$ m) wind speeds [contoured in solid (i.e., southwesterly) and dashed (i.e., northeasterly) in black starting from 4 and -4 m s^{-1}, respectively, at intervals of 4 m s^{-1}], and surface ($z = 2$ m) specific humidity (dotted shadings for ≥ 21 g kg^{-1}) that are taken along a rectangular area E–F through Wuxi and Nantong, as given in Fig. 7, valid during 1300–1600 LST 26 Jul 2018. Light green bars underneath the bottom frame represent water bodies. The blue stars denote the locations of the Wuxi and Nantong cities.

during 1300–1600 LST. Note that this time–distance cross section is plotted through cluster S and the Nantong city, rather than Haimen or Rudong, for the sake of qualitative understanding of the downstream discrete propagation of convective storms, in spite of the overpredicted rainfall amount at the Nantong city. It is evident that (i) higher MUCAPE (as high as 4000 J kg^{-1}) and specific humidity (greater than 21 g kg^{-1}) prior to the occurrence of rainfall (i.e., 1330 LST) are distributed in the coastal region due to the transport of moisture by sea breezes (cf. Figs. 11 and 6d); (ii) much less MUCAPE, though still with high moisture content, appears on the south of the Yangtze River by 1330 LST; (iii) the rapid reduction of MUCAPE after rainfall occurs; and (iv) relatively weak convergence and intense divergence near the Nantong city before and after the occurrence of rainfall, as indicated by the rightward-decreasing southwesterly flow, and the divergent northeasterly–southwesterly flows, respectively. Although CI occurs first on the downwind side of the Wuxi city near 1330 LST [note some delay from the CI to the generation of 1 mm (6 min)$^{-1}$], the MUCAPE and moisture fields on the south of the Yangtze River are less favorable than those on the north for the generation of intense convection and heavy rainfall. Apparently, these conditions help explain why heavy rainfall tends to take place on the north rather than south of the Yangtze River in the present case. Nevertheless, the southwesterly outflows so generated on the northeast of the Wuxi city, where light rainfall starts, (and the northwest of the Shanghai city; see Figs. 6b,d)

help trigger new convective cells, some of which are merged for the formation of cluster S by 1406 LST on the southern bank of the Yangtze River. As mentioned before, the water body, albeit narrow, appears to interrupt convective development, especially for the northward propagation of cluster S across the river, as indicated by much reduced rainfall rates in Fig. 11 and decreasing rainfall amounts toward the river in both the observations and simulation (cf. Figs. 1b and 7). However, the (cold) southwesterly outflows generated by cluster S interacting with the moist easterly flows, which are enhanced by outflows from convective storms near Haimen (Fig. 6f), induce pronounced surface convergence near the Nantong city, leading to the generation of more rainfall than the observed there. Sustained (area-averaged) rainfall rates of 5–7 mm (6 min)$^{-1}$ are seen during the period of 1430–1515 LST, which are more or less consistent with the accumulated heavy rainfall coverage shown in Fig. 7.

5. Sensitivity simulations

Since the timings and locations of the CI and associated rainfall distributions and centers are reasonably simulated, the model simulation can be used as a control simulation (CNTL experiment) to perform a series of sensitivity simulations in order to analyze to what extent the UHI effects of the city belt versus Nantong account for the generation of heavy rainfall on the north of the Yangtze River.

TABLE 1. Description of experiment design.

Expt	Description
CNTL	1) Include apparent UHI effects over the YRD region in the initial conditions 2) Observation nudging of the UHI effects during 0200–0800 LST 26 Jul 3) Single-layer urban canopy model
NoUrban	1) Replace urban and builtup land uses by croplands within D01, D02, and D03 2) Remove the apparent UHI effects over the YRD region in the initial conditions 3) Turn off observation nudging 4) Turn off the single-layer urban canopy model
NTOff	1) Replace urban and builtup land uses by croplands only over the Nantong region 2) Remove the UHI effects over the Nantong region in the initial conditions 3) Observation nudging of the UHI effects within D03 except for the Nantong region 4) Single-layer urban canopy model
NTOn	1) Replace urban and builtup land uses by croplands except for the Nantong region 2) Apparent UHI effects only over the Nantong region in the initial conditions 3) Observation nudging within D03 only for the Nantong region 4) Single-layer urban canopy model

a. Experimental design

Three sensitivity simulations are conducted to examine the UHI effects of the city belt versus Nantong on the generation of heavy rainfall (Table 1). They are done by removing the urban impacts of different regions with the corresponding model settings changed while keeping all the other settings identical to those used in the control simulation. In the first simulation, the urban and builtup land uses over all of the three domains are replaced by croplands that are as same as those over the neighboring rural regions in order to test the overall impact of urbanization on the rainfall over the YRD region, hereafter referred to as the NoUrban experiment. To eliminate the influences of the UHI effects from the initial conditions, warm anomalies of the FNL reanalysis from the surface layer to 850 hPa over the YRD urban regions (119.00°–122.50°E, 29.75°–32.50°N) are removed. In addition, the observed surface meteorological fields are no longer nudged, and the single-layer urban canopy model is turned off. In the second simulation, the roles of the city belt in determining the heavy rainfall over the Nantong region are examined by replacing the urban and its nearby builtup land uses over the Nantong region with croplands, which is referred to as the NTOff experiment. Moreover, the initial UHI effects over the Nantong region are removed, and the observation nudging of the UHI effects for the Nantong region is turned off. In the third simulation, the urban impact of Nantong on the development of heavy rainfall over its own territory (i.e., NTOn) is examined by replacing the urban and its nearby builtup land uses on Nantong's upstream, including the city belt, with croplands. The associated UHI effects along the city belt in the model initial conditions are also removed.

b. Effects of regional urbanization

By replacing all of the urban and builtup land uses over the three domains with croplands (i.e., NoUrban), the model produces quite a different rainfall distribution from that in CNTL

(cf. Figs. 12a and 7). Specifically, significant rainfall occurs mainly on the west of Hangzhou as a result of complex topography. In contrast, a few weak rainfall spots of <30 mm are generated along the Yangtze River banks, and over areas between Hangzhou and Shanghai. Of particular relevance is that little rainfall occurs over the plain area on the north of Hangzhou, and along the Shanghai–SXC city belt as in CNTL. In addition, no CI is triggered by noon over the urban regions as in CNTL, despite the presence of similar surface flow patterns in the two simulations (not shown). Only a few scattered storms develop along the Yangtze River banks later, e.g., by 1406 LST (Fig. 12b), which coincide closely with the surface convergence zone. Although a storm propagates to Haimen from the south, it produces less than 10-mm rainfall with little evidence of cold downdraft air as in CNTL. Moreover, the CIs of all the storms are significantly delayed, as compared to those in CNTL. The distribution and evolution of the convergence zone represent onshore movement of sea breezes interacting with lake- and river-induced circulations that contribute to the afternoon CI in the north of the YRD region. This result indicates that the sea/lake/river breezes could trigger some scattered and short-lived storms during the afternoon hours along the Yangtze River banks, including Nantong, but they could not produce organized convective storms with heavy rainfall over the coastal Nantong region. On the other hand, this result helps explain why heavy rainfall occurs over Nantong, rather than during the course of the propagating storms, in both the observations and CNTL, because of the enhanced convergence and more moisture available from the maritime PBL, as also mentioned in section 4.

To help further understand the role of the city belt in triggering CI, Fig. 13a shows the differenced fields of near-surface temperature and winds between CNTL and NoUrban (i.e., CNTL minus NoUrban) at 1030 LST, i.e., CI just begins along the city belt. Apparently, the near-surface temperature increases more than 0.5°C over the YRD region under the influences of urbanization, with sharp increases of more than 1.0°C at the urban
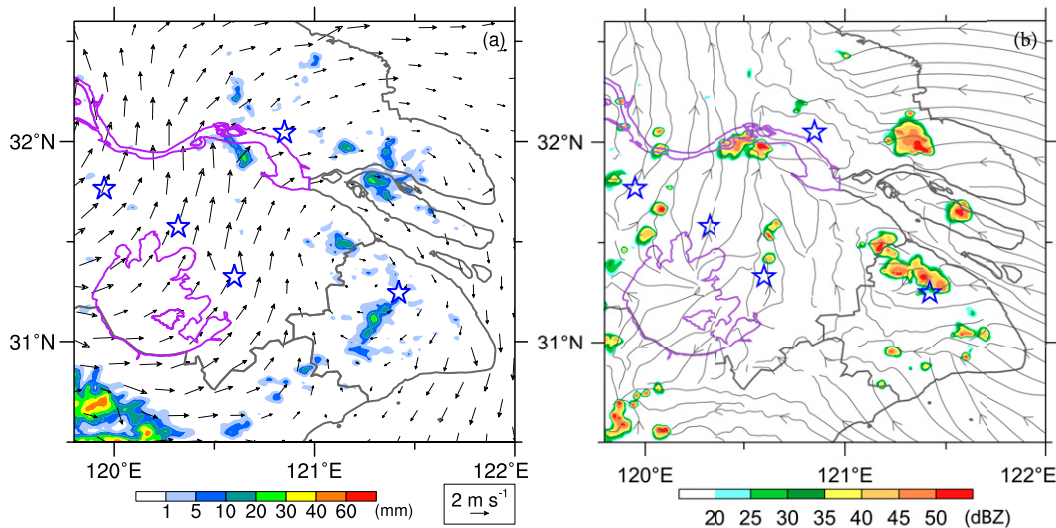
FIG. 12. (a) As in Fig. 7, but for NoUrban. (b) As in Fig. 6f, but for NoUrban at 1406 LST 26 Jul 2018.

areas (e.g., the Shanghai, Suzhou, and Nantong cities). The large area of "warmer air" downstream from the city belt, which is distinct from little changes in the upstream near-surface temperature, represents the downstream cascade of the UHI effects (Zhang et al. 2009). The differenced near-surface wind vectors show the presence of convergence toward urban centers. After all, the changes in both the surface temperature and winds reflect the UHI and urban canopy effects of the city belt and Nantong (Shepherd 2005; Zhang 2020). A south–north vertical cross section through Shanghai shows that the PBL warm anomalies at the Shanghai city disappear in NoUrban, with the 308–309-K isentropic contours nearly flat northward to Nantong, as compared to those in CNTL (cf. Figs. 13b and 9b). Note, however, that the 308–309-K isentropic contours over Nantong are as elevated as those seen in CNTL, which is consistent with the subsequent CI of a convective storm near Haimen (Fig. 12b). These elevated isentropic contours result likely from the lifting of the lower-level convergence associated with sea breezes, as suggested by favorable upward motion ahead of the sea-breeze front (Fig. 13b). The above results confirm the importance of warm anomalies and surface convergence in triggering CI along the city belt, the enhanced UHI effects toward Nantong and beyond in the downstream propagation of the convective storms initiated at the city belt, and the enhanced convergence of sea breezes in producing the heavy rainfall event over the coastal region.

c. Effects of upstream versus local urbanization

As mentioned earlier, upstream urbanization may exacerbate the UHI effects and cascade downwind (Zhang et al. 2009), which tends to destabilize atmospheric columns downstream. Nantong, a developing city with several well-developed cities to its south, is located on the east coast and downstream of the urban agglomerations in summer. To explore to what extent Nantong itself and the upstream cities affect its local heavy rainfall, two sensitivity

simulations are conducted by removing the urban and builtup land uses associated with Nantong and the city belt, respectively.

By treating Nantong's urban area as a rural area (NTOff), the model produces some notable but relatively small differences in the distribution and amount of rainfall over the coastal Nantong region, as compared to those in CNTL (cf. Figs. 14a and 7). For example, the rainfall distribution around the Nantong city changes from a circular to a south-north-oriented pattern extending to near Rudong, and the rainfall center at Haimen appears closer to the coastline. They could be attributed to the interaction of propagating storms with the low-level convergence zone associated with the sea-breeze front (cf. Figs. 14a and 12b). Turning off Nantong's urban impacts also produces slightly less rainfall near the Nantong city, Haimen, and over regions along the Yangtze River banks. There are little differences in the near-surface temperature and winds between NTOff and CNTL, except with a warm anomaly of less than 1.0°C and weak convergence nearby the city center under the influence of urbanization (Fig. 14c). This sensitivity simulation indicates that Nantong's UHI effects do help destabilize to some extent atmospheric columns and enhance low-level convergence for the development of more organized convective storms.

In contrast, treating the urban regions along the city belt as rural (i.e., NTOn) produces subtle differences in the total rainfall distribution and amount from those in CNTL (cf. Figs. 14b and 7). In particular, this simulation with only Nantong's urbanization effects does not produce heavy rainfall in the northern YRD region. Instead, only a few scattered rainfall centers of 10–30 mm take place outside of the Nantong city. Moreover, little rainfall occurs over a large area from the city belt to Nantong, and along the coastal regions from the southern Shanghai to Haimen. The differenced near-surface temperature and winds between CNTL and NTOn show that warm anomalies occur not only along the city belt but also over the coastal Nantong region, where wind vectors (i.e., sea breezes) strengthen in the presence of the city belt (Fig. 14d). This simulation indicates
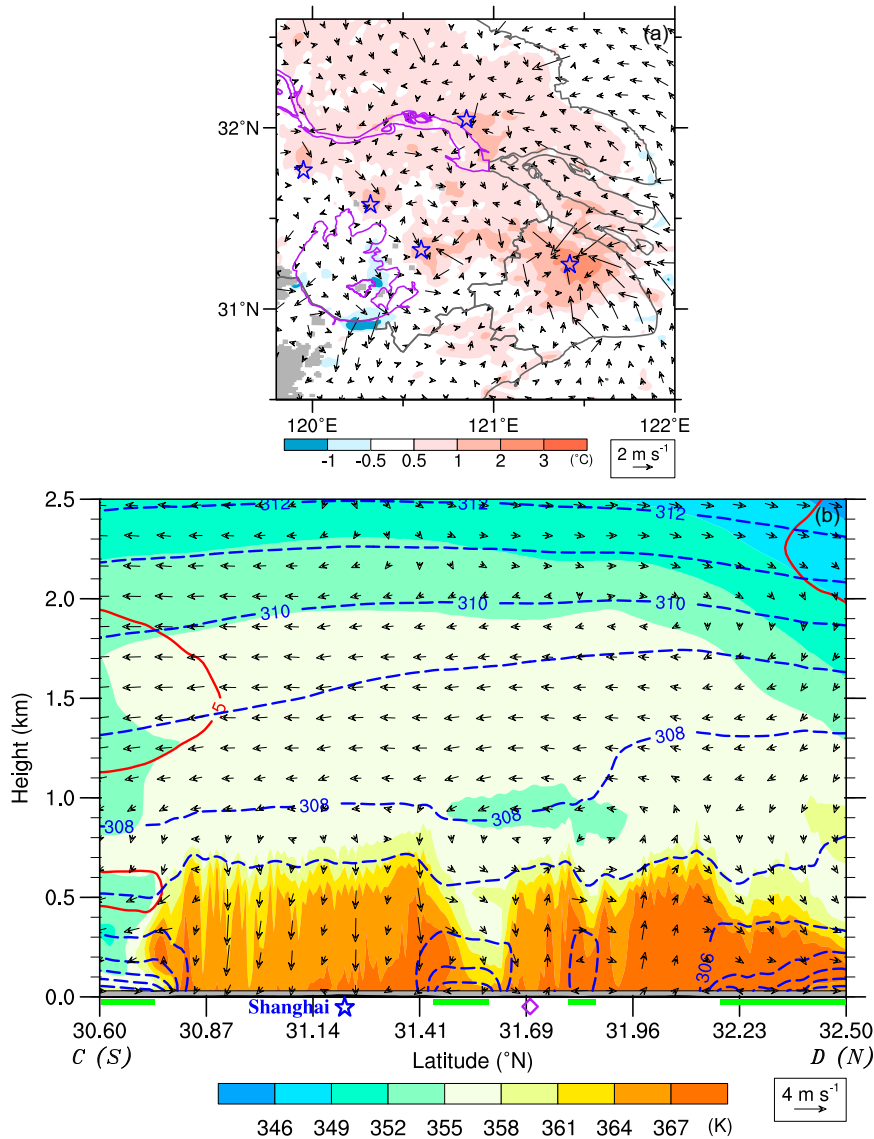
FIG. 13. (a) Differences in the fields of near-surface ($z = 100$ m) temperature (shaded; °C) and horizontal winds between CNTL and NoUrban at 1030 LST. (b) As in Fig. 9b, but for NoUrban.

the dominant roles of the city belt in determining the heavy rainfall event over the Nantong region, including Haimen and Rudong. Nantong's urban impacts could produce some scattered storms with the aid of sea breezes, but they are too weak to trigger more organized, heavy-rain-producing storms.

To help understand the different convective behaviors in the vicinity of Nantong among the different simulations, Fig. 15 compares soundings taken at the Nantong city prior to CI (i.e., 1300 LST) from the four simulations. All the simulations produce a well-mixed PBL up to 850 hPa, but that Exp. CNTL has the warmest (except in the lowest 50-hPa layer) and moistest PBL with saturation already occurring in the 850–800-hPa layer by 1300 LST, whereas NoUrban has the coldest and driest PBL.

As mentioned in section 4, this saturated layer in CNTL results from the advection of warm and moist air by the southwesterly flow prior to 1300 LST (cf. Figs. 10c and 15) and low-level convergence between southerly cold outflows from Shanghai and the city belt and northeasterly (moist) sea breezes (cf. Figs. 15, 6d, and 11). Of interest is that the northeasterly sea breezes in CNTL are "retreated" eastward and replaced by southwesterly to southeasterly flows when the builtup land uses are replaced by croplands, i.e., in NoUrban, NTOn, and NTOff. This indicates that the enhanced UHI effects in the coastal region increase the land–sea temperature contrast and thus strengthen the sea breezes, thereby leading to transport of more moisture into the PBL near Nantong.
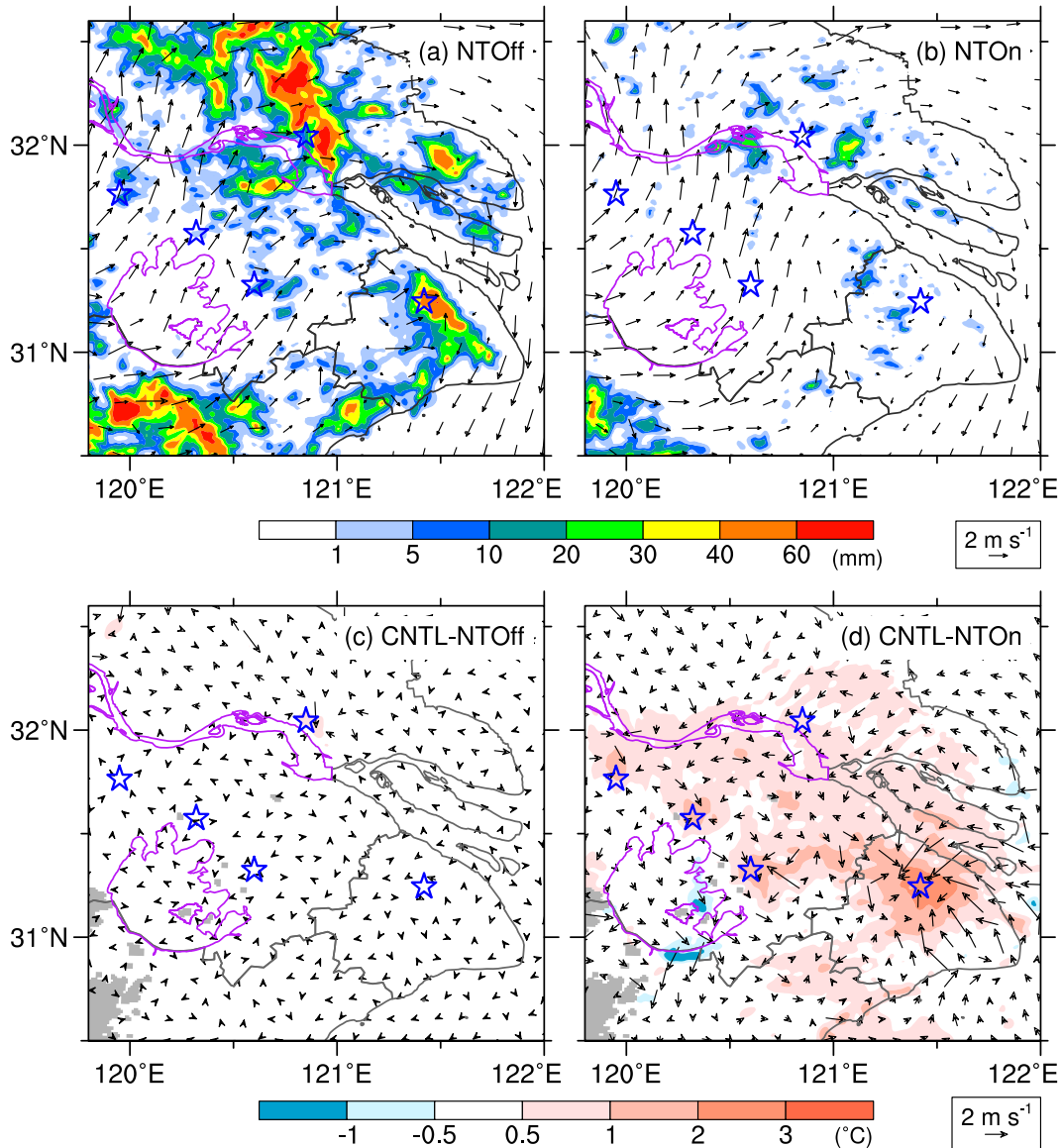
FIG. 14. (a),(b) As in Fig. 7, but for NTOff and NTOn, respectively. (c),(d) As in Fig. 13a, but for differences between CNTL and NTOff in (c) and between CNTL and NTOn in (d).

6. Summary and conclusions

In this study, the impacts of urbanization on the CI and subsequent heavy rainfall under the influences of sea and lake breezes and complex surface conditions over the YRD region during the hours of 0800–1600 LST 26 July 2018 are examined using a series of cloud-permitting simulations with the finest grid spacing of 1 km. Observations show that this heavy rainfall event took place under a weak-gradient environment with weak flows, controlled by a subtropical high centered over the northwest Pacific Ocean and weak southwesterly monsoonal flows. CI occurred on the downstream sides of the Shanghai–SXC city belt with the aid of sea and lake breezes during the morning hours, but heavy rainfall centers appeared in the afternoon at

Haimen (69.3 mm) and Rudong (89.2 mm), which are located over the coastal Nantong region about 70–100 km downwind from the city belt.

In general, a control simulation, initialized with the observation nudging of surface temperature, moisture, and winds over the YRD region, reproduces reasonably well the observed UHI effects at the multiple urban centers by 1000 LST, CI shortly after on the downstream sides of the city belt and the subsequent merging to convective clusters during their downstream propagation, and the ultimate generation of heavy rainfall centers near Haimen, Rudong and the other locations over the Nantong region. Specifically, distinct warm anomalies in the lowest 500–1000-m layer are seen at Shanghai and Suzhou with the
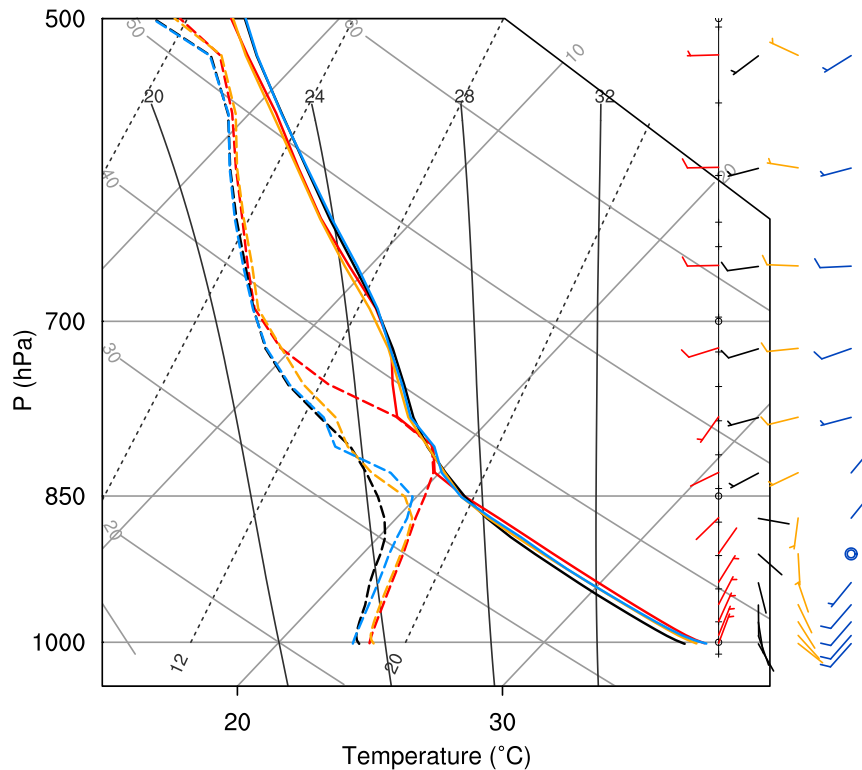
FIG. 15. Simulated soundings at the Nantong city from CNTL (red), NoUrban (black), NTOff (orange), and NTOn (blue), valid at 1300 LST 26 Jul 2018. A full barb is 4 m s^{-1}.

ambient convergence along the fronts of sea and lake breezes, leading to the CI. Some convective cells dissipate shortly after their formation, whereas the others are merged into convective clusters. Results show that the PBL depth increases from the Shanghai–SXC city belt downstream to Nantong, due to the advection of monsoonal warm–moist air and the UHI effects, providing favorable conditions for the initiation of new convection at the convectively generated outflow boundaries associated with weakening storms. The heavy rainfall event is generated by locally formed convective clusters over the coastal Nantong region where atmospheric columns are more potentially unstable with higher moisture content under the influences of sea breezes. The control simulation (and observations) also shows the impact of the Yangtze River on the interruption of convective development associated with the northward propagating convective cells/clusters due to the presence of a shallow stable layer over the water surface.

Sensitivity simulations are performed to examine to what extent the UHI effects of the city belt versus Nantong account for the subsequent generation of heavy rainfall over the coastal Nantong region. Results show little rainfall over the plain area on the north of Hangzhou, including the Shanghai–SXC city belt, after replacing urban and builtup land uses by croplands over the YRD region. The coastal Nantong region only experiences small amount of rainfall associated with sea breezes. By comparison, the downstream propagation of the UHI effects from the city belt increases the thermal contrasts across the

coastline and the associated onshore moisture convergence, thereby assisting in the generation of heavier rainfall over the coastal Nantong region. A comparison of two contrasting sensitivity simulations (i.e., NTOff and NTOn) illustrates that only slight reductions in rainfall occur near the Nantong city, Haimen, and over regions along the Yangtze River banks when Nantong is treated as a rural area, whereas only small amount of rainfall appears in the northern YRD when the Shanghai-SXC city belt is treated as rural areas. These results indicate that Nantong's UHI effects do help destabilize to some extent atmospheric columns and enhance low-level convergence for the generation of some rainfall, but they do not contribute significantly to the heavy rainfall event over the coastal Nantong region.

In conclusion, we may state that (i) the UHI effects of the Shanghai-SXC city belt under the influences of sea and lake breezes facilitate CI at some preferred locations; (ii) the downstream advection of the UHI effects in the presence of the favorable monsoonal warm–moist airstream assists in the subsequent downstream propagation of convective storms, which are initiated near the city belt and then merged into convective clusters, to the north of the Yangtze River; and (iii) the heavy rainfall event over the coastal Nantong region is generated by local convective clusters that are embedded in an environment in which the atmosphere is more potentially unstable with ample moisture under the influences of sea breezes. The above results support the recent IPCC (2021) Sixth Assessment Report, stating that urbanization has contributed to "increases in mean and

extreme precipitation over and downwind of the city, especially in the afternoon and early evening (*medium confidence*)." Recognizing some limitations and weaknesses with the present case study, the above findings not only help explain why more rainfall tends to take place on the downwind side of major cities, but also have important implications to the understanding of the UHI effects on the CI and downstream propagation of convective storms, leading to the eventual generation of heavy rainfall at locations where the regional environment is favorable.

Data availability statement. The NCEP-FNL reanalysis data can be downloaded from online archive system at https://rda.ucar.edu/datasets/ds083.3/. The 1-km grid spacing land-use dataset from RESDC is available online at http://www.resdc.cn/data.aspx?DATAID=98. Due to CMA's data policy, observational data of AWSs and radars are not publicly available. Simulation output supporting the findings of this study is available on request from the authors.

REFERENCES

Bélair, S., and J. Mailhot, 2001: Impact of horizontal resolution on the numerical simulation of a midlatitude squall line: Implicit versus explicit condensation. *Mon. Wea. Rev.*, **129**, 2362–2376, https://doi.org/10.1175/1520-0493(2001)129<2362:IOHROT>2.0.CO;2.

Changnon, S. A., Jr., 1968: The LaPorte weather anomaly—Fact or fiction. *Bull. Amer. Meteor. Soc.*, **49**, 4–11, https://doi.org/10.1175/1520-0477-49.1.4.

——, 1969: Recent studies of urban effects on precipitation in the United States. *Bull. Amer. Meteor. Soc.*, **50**, 411–421, https://doi.org/10.1175/1520-0477-50.6.411.

——, R. G. Semonin, A. H. Auer, R. R. Braham Jr., and J. M. Hales 1981: *METROMEX: A Review and Summary. Meteor. Monogr.*, No. 40, Amer. Meteor. Soc., 81 pp.

Chen, F., and Coauthors, 2011: The integrated WRF/urban modeling system: Development, evaluation, and applications to urban environmental problems. *Int. J. Climatol.*, **31**, 273–288, https://doi.org/10.1002/joc.2158.

——, M. Wu, M. Dong, and B. Yu, 2022: Comparison of the impacts of topography and urbanization on an extreme rainfall event in the Hangzhou Bay region. *J. Geophys. Res. Atmos.*, **127**, e2022JD037060, https://doi.org/10.1029/2022JD037060.

Chen, Y., P. Zhai, and B. Zhou, 2018: Detectable impacts of the past half-degree global warming on summertime hot extremes in China. *Geophys. Res. Lett.*, **45**, 7130–7139, https://doi.org/10.1029/2018GL079216.

Doan, Q.-V., A. Dipankar, A. Simón-Moral, C. Sanchez, V. Prasanna, M. Roth, and X.-Y. Huang, 2021: Urban-induced modifications to the diurnal cycle of rainfall over a tropical city. *Quart. J. Roy. Meteor. Soc.*, **147**, 1189–1201, https://doi.org/10.1002/qj.3966.

Dou, J., Y. Wang, R. Bornstein, and S. Miao, 2015: Observed spatial characteristics of Beijing urban climate impacts on summer thunderstorms. *J. Appl. Meteor. Climatol.*, **54**, 94–105, https://doi.org/10.1175/JAMC-D-13-0355.1.

IPCC, 2021: *Climate Change 2021: The Physical Science Basis.* Cambridge University Press, 2391 pp., https://doi.org/10.1017/9781009157896.

Janjić, Z. I., 1994: The step–mountain eta coordinate model: Further developments of the convection, viscous sublayer, and turbulence closure schemes. *Mon. Wea. Rev.*, **122**, 927–945, https://doi.org/10.1175/1520-0493(1994)122<0927:TSMECM>2.0.CO;2.

——, 2002: Nonsingular implementation of the Mellor-Yamada Level 2.5 scheme in the NCEP Meso Model. NCEP Office Note 437, 61 pp., http://www.emc.ncep.noaa.gov/officenotes/newernotes/on437.pdf.

Jiang, X., Y. Luo, D.-L. Zhang, and M. Wu, 2020: Urbanization enhanced summertime extreme hourly precipitation over the Yangtze River Delta. *J. Climate*, **33**, 5809–5826, https://doi.org/10.1175/JCLI-D-19-0884.1.

Kain, J. S., 2004: The Kain–Fritsch convective parameterization: An update. *J. Appl. Meteor. Climatol.*, **43**, 170–181, https://doi.org/10.1175/1520-0450(2004)043<0170:TKCPAU>2.0.CO;2.

Kingfield, D. M., K. M. Calhoun, K. M. de Beurs, and G. M. Henebry, 2018: Effects of city size on thunderstorm evolution revealed through a multiradar climatology of the central United States. *J. Appl. Meteor. Climatol.*, **57**, 295–317, https://doi.org/10.1175/JAMC-D-16-0341.1.

Kishtawal, C. M., D. Niyogi, M. Tewari, R. A. Pielke, and J. M. Shepherd, 2010: Urbanization signature in the observed heavy rainfall climatology over India. *Int. J. Climatol.*, **30**, 1908–1916, https://doi.org/10.1002/joc.2044.

Lacono, M. J., J. S. Delamere, E. J. Mlawer, M. W. Shephard, S. A. Clough, and W. D. Collins, 2008: Radiative forcing by long-lived greenhouse gases: Calculations with the AER radiative transfer models. *J. Geophys. Res.*, **113**, D13103, https://doi.org/10.1029/2008JD009944.

Lei, M., D. Niyogi, C. Kishtawal, R. A. Pielke, A. Beltrán-Przekurat, T. E. Nobis, and S. S. Vaidya, 2008: Effect of explicit urban land surface representation on the simulation of the 26 July 2005 heavy rain event over Mumbai India. *Atmos. Chem. Phys.*, **8**, 5975–5995, https://doi.org/10.5194/acp-8-5975-2008.

Li, H., X. Cui, and D.-L. Zhang, 2017a: Sensitivity of the initiation of an isolated thunderstorm over the Beijing metropolitan region to urbanization, terrain morphology and cold outflows. *Quart. J. Roy. Meteor. Soc.*, **143**, 3153–3164, https://doi.org/10.1002/qj.3169.

——, ——, and ——, 2017b: On the initiation of an isolated heavy-rain-producing storm near the central urban area of the Beijing metropolitan region. *Mon. Wea. Rev.*, **145**, 181–197, https://doi.org/10.1175/MWR-D-16-0115.1.

——, ——, and ——, 2017c: A statistical analysis of hourly heavy rainfall events over the Beijing metropolitan region during the warm seasons of 2007–2014. *Int. J. Climatol.*, **37**, 4027–4042, https://doi.org/10.1002/joc.4983.

Li, M., Y. Luo, D.-L. Zhang, M. Chen, C. Wu, J. Yin, and R. Ma, 2021: Analysis of a record-breaking rainfall event associated with a monsoon coastal megacity of South China using multisource

data. *IEEE Trans. Geosci. Remote Sens.*, **59**, 6404–6414, https://doi.org/10.1109/TGRS.2020.3029831.

Li, Y., and Coauthors, 2020: Strong intensification of hourly rainfall extremes by urbanization. *Geophys. Res. Lett.*, **47**, e2020GL088758, https://doi.org/10.1029/2020GL088758.

Li, Z., X. Deng, F. Wu, and S. S. Hasan, 2015: Scenario analysis for water resources in response to land use change in the middle and upper reaches of the Heihe River basin. *Sustainability*, **7**, 3086–3108, https://doi.org/10.3390/su7033086.

Liang, P., and Y. Ding, 2017: The long-term variation of extreme heavy precipitation and its link to urbanization effects in Shanghai during 1916–2014. *Adv. Atmos. Sci.*, **34**, 321–334, https://doi.org/10.1007/s00376-016-6120-0.

Lim, K.-S. S., and S.-Y. Hong, 2010: Development of an effective double-moment cloud microphysics scheme with prognostic cloud condensation nuclei (CCN) for weather and climate models. *Mon. Wea. Rev.*, **138**, 1587–1612, https://doi.org/10.1175/2009MWR2968.1.

Liu, B., J. Guo, W. Gong, L. Shi, Y. Zhang, and Y. Ma, 2020: Characteristics and performance of wind profiles as observed by the radar wind profiler network of China. *Atmos. Meas. Tech.*, **13**, 4589–4600, https://doi.org/10.5194/amt-13-4589-2020.

Liu, J., and D. Niyogi, 2019: Meta-analysis of urbanization impact on rainfall modification. *Sci. Rep.*, **9**, 7301, https://doi.org/10.1038/s41598-019-42494-2.

——, and Coauthors, 2014: Spatiotemporal characteristics, patterns, and causes of land-use changes in China since the late 1980s. *J. Geogr. Sci.*, **24**, 195–210, https://doi.org/10.1007/s11442-014-1082-6.

Liu, Y., and Coauthors, 2008: The operational mesogamma-scale analysis and forecast system of the U.S. army test and evaluation command. Part I: Overview of the modeling system, the forecast products, and how the products are used. *J. Appl. Meteor. Climatol.*, **47**, 1077–1092, https://doi.org/10.1175/2007JAMC1653.1.

Luo, Y., M. Wu, F. Ren, J. Li, and W.-K. Wong, 2016: Synoptic situations of extreme hourly precipitation over China. *J. Climate*, **29**, 8703–8719, https://doi.org/10.1175/JCLI-D-16-0057.1.

Mesinger, F., 1993: Forecasting upper tropospheric turbulence within the framework of the Mellor-Yamada 2.5 closure. Research Activities in Atmospheric and Oceanic Models, WMO 18, CAS/JSC WANG Press, 4.28–4.29.

Miao, S., F. Chen, Q. Li, and S. Fan, 2011: Impacts of urban processes and urbanization on summer precipitation: A case study of heavy rainfall in Beijing on 1 August 2006. *J. Appl. Meteor. Climatol.*, **50**, 806–825, https://doi.org/10.1175/2010JAMC2513.1.

Niyogi, D., P. Pyle, M. Lei, S. P. Arya, C. M. Kishtawal, M. Shepherd, F. Chen, and B. Wolfe, 2011: Urban modification of thunderstorms: An observational storm climatology and model case study for the Indianapolis urban region. *J. Appl. Meteor. Climatol.*, **50**, 1129–1144, https://doi.org/10.1175/2010JAMC1836.1.

Rotunno, R., J. B. Klemp, and M. L. Weisman, 1988: A theory for strong, long-lived squall lines. *J. Atmos. Sci.*, **45**, 463–485, https://doi.org/10.1175/1520-0469(1988)045<0463:ATFSLL>2.0.CO;2.

Shepherd, J. M., 2005: A review of current investigations of urban-induced rainfall and recommendations for the future. *Earth Interact.*, **9**, https://doi.org/10.1175/EI156.1.

——, and S. J. Burian, 2003: Detection of urban induced rainfall anomalies in a major coastal city. *Earth Interact.*, **7**, https://doi.org/10.1175/1087-3562(2003)007<0001:DOUIRA>2.0.CO;2.

Stauffer, D. R., and N. L. Seaman, 1990: Use of four-dimensional data assimilation in a limited-area mesoscale model. Part I: Experiments with synoptic-scale data. *Mon. Wea. Rev.*, **118**, 1250–1277, https://doi.org/10.1175/1520-0493(1990)118<1250:UOFDDA>2.0.CO;2.

——, and ——, 1994: Multiscale four-dimensional data assimilation. *J. Appl. Meteor.*, **33**, 416–434, https://doi.org/10.1175/1520-0450(1994)033<0416:MFDDA>2.0.CO;2.

——, ——, and F. S. Binkowski, 1991: Use of four-dimensional data assimilation in a limited-area mesoscale model. Part II: Effects of data assimilation within the planetary boundary layer. *Mon. Wea. Rev.*, **119**, 734–754, https://doi.org/10.1175/1520-0493(1991)119<0734:UOFDDA>2.0.CO;2.

Sun, X., Y. Luo, X. Gao, M. Wu, M. Li, L. Huang, D.-L. Zhang, and H. Xu, 2021: On the localized extreme rainfall over the Great Bay area in South China with complex topography and strong UHI effects. *Mon. Wea. Rev.*, **149**, 2777–2801, https://doi.org/10.1175/MWR-D-21-0004.1.

Wan, H., Z. Zhong, X. Yang, and X. Li, 2013: Impact of city belt in Yangtze River Delta in China on a precipitation process in summer: A case study. *Atmos. Res.*, **125–126**, 63–75, https://doi.org/10.1016/j.atmosres.2013.02.004.

Wu, M., Y. Luo, F. Chen, and W. K. Wong, 2019: Observed link of extreme hourly precipitation changes to urbanization over coastal South China. *J. Appl. Meteor. Climatol.*, **58**, 1799–1819, https://doi.org/10.1175/JAMC-D-18-0284.1.

Yao, X., J. Ma, D.-L. Zhang, and L. Yan, 2020: A 33-yr mei-yu-season climatology of shear lines over the Yangtze–Huai River basin in eastern China. *J. Appl. Meteor. Climatol.*, **59**, 1125–1137, https://doi.org/10.1175/JAMC-D-19-0229.1.

Yau, M. K., Y. Liu, D.-L. Zhang, and Y. Chen, 2004: A multiscale numerical study of Hurricane Andrew (1992). Part VI: Small-scale inner-core structures and wind streaks. *Mon. Wea. Rev.*, **132**, 1410–1433, https://doi.org/10.1175/1520-0493(2004)132<1410:AMNSOH>2.0.CO;2.

Yin, J., D.-L. Zhang, Y. Luo, and R. Ma, 2020: On the extreme rainfall event of 7 May 2017 over the coastal city of Guangzhou. Part I: Impacts of urbanization and orography. *Mon. Wea. Rev.*, **148**, 955–979, https://doi.org/10.1175/MWR-D-19-0212.1.

Yu, R., J. Li, W. Yuan, and H. Chen, 2010: Changes in characteristics of late-summer precipitation over eastern China in the past 40 years revealed by hourly precipitation data. *J. Climate*, **23**, 3390–3396, https://doi.org/10.1175/2010JCLI3454.1.

Zhang, D., and R. A. Anthes, 1982: A high-resolution model of the planetary boundary layer—Sensitivity tests and comparisons with SESAME-79 data. *J. Appl. Meteor. Climatol.*, **21**, 1594–1609, https://doi.org/10.1175/1520-0450(1982)021<1594:AHRMOT>2.0.CO;2.

Zhang, D.-L., 2020: Rapid urbanization and more extreme rainfall events. *Sci. Bull.*, **65**, 516–518, https://doi.org/10.1016/j.scib.2020.02.002.

——, Y.-X. Shou, and R. R. Dickerson, 2009: Upstream urbanization exacerbates urban heat island effects. *Geophys. Res. Lett.*, **36**, L24401, https://doi.org/10.1029/2009GL041082.

——, ——, ——, and F. Chen, 2011: Impact of upstream urbanization on the urban heat island effects along the Washington–Baltimore corridor. *J. Appl. Meteor. Climatol.*, **50**, 2012–2029, https://doi.org/10.1175/JAMC-D-10-05008.1.

Zhang, N., and Y. Chen, 2014: A case study of the upwind urbanization influence on the urban heat island effects along the Suzhou–Wuxi corridor. *J. Appl. Meteor. Climatol.*, **53**, 333–345, https://doi.org/10.1175/JAMC-D-12-0219.1.

Zhong, S., and X.-Q. Yang, 2015: Ensemble simulations of the urban effect on a summer rainfall event in the great Beijing metropolitan area. *Atmos. Res.*, **153**, 318–334, https://doi.org/10.1016/j.atmosres.2014.09.005.

Zhu, B., H. Kang, T. Zhu, J. Su, X. Hou, and J. Gao, 2015: Impact of Shanghai urban land surface forcing on downstream city ozone chemistry. *J. Geophys. Res. Atmos.*, **120**, 4340–4351, https://doi.org/10.1002/2014JD022859.